ACS SENSORS

pubs.acs.org/acssensors

Article

Dynamic Laser Speckle Imaging Meets Machine Learning to Enable Rapid Antibacterial Susceptibility Testing (DyRAST)

Keren Zhou, Chen Zhou, Anjali Sapre, Jared Henry Pavlock, Ashley Weaver, Ritvik Muralidharan, Josh Noble, Taejung Chung, Jasna Kovac, Zhiwen Liu,* and Aida Ebrahimi*

Cite This: *ACS Sens.* 2020, 5, 3140–3149

Read Online

ACCESS | Metrics & More | Article Recommendations | Supporting Information

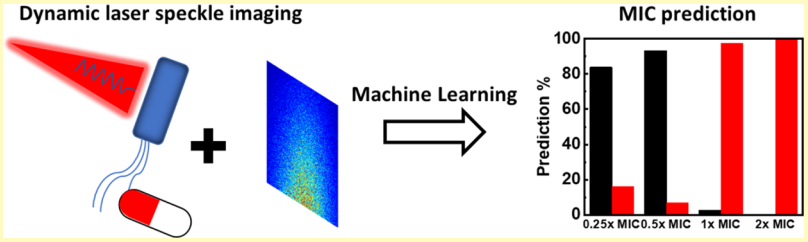

ABSTRACT: Rapid antibacterial susceptibility testing (RAST) methods are of significant importance in healthcare, as they can assist caregivers in timely administration of the correct treatments. Various RAST techniques have been reported for tracking bacterial phenotypes, including size, shape, motion, and redox state. However, they still require bulky and expensive instruments—which hinder their application in resource-limited environments—and/or utilize labeling reagents which can interfere with antibiotics and add to the total cost. Furthermore, the existing RAST methods do not address the potential gradual adaptation of bacteria to antibiotics, which can lead to a false diagnosis. In this work, we present a RAST approach by leveraging machine learning to analyze time-resolved dynamic laser speckle imaging (DLSI) results. DLSI captures the change in bacterial motion in response to antibiotic treatments. Our method accurately predicts the minimum inhibitory concentration (MIC) of ampicillin and gentamicin for a model strain of *Escherichia coli* (*E. coli* K-12) in 60 min, compared to 6 h using the currently FDA-approved phenotype-based RAST technique. In addition to ampicillin (a β-lactam) and gentamicin (an aminoglycoside), we studied the effect of ceftriaxone (a third-generation cephalosporin) on *E. coli* K-12. The machine learning algorithm was trained and validated using the overnight results of a gold standard antibacterial susceptibility testing method enabling prediction of MIC with a similarly high accuracy yet substantially faster.

KEYWORDS: *antibacterial susceptibility testing, phenotype, bacteria, laser speckle imaging, machine learning*

Antimicrobial resistance (AMR) is among the most serious health threats of all time. Antimicrobial-resistant pathogens cause an estimated 2.8 million infections and 35,000 deaths per year in the United States.[1] The fatality rate due to antimicrobial-resistant infections is expected to reach 10 million per year by 2050 if the expansion of AMR is not effectively mitigated.[2] Misuse and overuse of broad-spectrum antibiotics due to the absence of reliable and accurate rapid antibacterial susceptibility testing (RAST) is contributing to the spread of AMR infections. Gold standard antibacterial susceptibility testing (AST) techniques, including disk diffusion and broth microdilution (BMD), take over 16 h to complete which limits their utility in cases of severe sepsis.[3,4] The EUCAST developed a RAST method in 2019 that can determine the minimum inhibitory concentration (MIC) results for seven species within 4−8 h based on the disk diffusion method.[5] Further development of accurate RAST that produces results concordant with gold standard methods is therefore critically needed to speed up AST to support data-informed antibiotic prescription and improve patient treatment outcomes.

A series of molecular and phenotypic technologies has recently been developed for RAST and detection of AMR. Molecular methods rely on the detection of target nucleic acid sequence markers to determine and predict antibiotic resistance.[6] Amplification of target DNA using polymerase chain reaction (PCR),[7] isothermal recombinase polymerase amplification,[8] or loop-mediated isothermal amplification (LAMP)[9,10] combined with fluorescence detection[11] can produce the results within an hour. Because of diverse genetic resistance determinants that do not have sufficient correlation

Received: June 19, 2020
Accepted: September 18, 2020
Published: September 18, 2020

with resistance phenotypes, culture-independent AST testing cannot be broadly applied to all pathogens without extensive prior knowledge of their biology and underlying genetics. Furthermore, molecular methods still fail to detect resistance in cases where novel resistance mechanisms have not yet been characterized.[12−14]

Compared to molecular methods, phenotype-based ASTs in many cases provide information that is more relevant to clinical outcomes. Among different phenotypic methods, Accelerate Pheno (Accelerate Diagnostics, Inc., Tucson, AZ, USA) is currently the only FDA-approved RAST technique. This method measures morphokinetic cellular changes that occur due to exposure to antibiotics. Accelerate Pheno combines fluorescence in situ hybridization and automated microscopic imaging to identify bacteria.[15] Baltekin et al. used single-cell imaging in a microfluidic cartridge with phase-contrast microscopy and identified resistant bacteria within 30 min.[16] A method reported by Schoepp et al. has further improved the time-to-results by determining the antimicrobial susceptibility of *Escherichia coli* directly from clinical urine samples in 30 min.[9] Their technique, coupled with digital LAMP, measures microbial growth based on quantification of nucleic acids using quantitative PCR. One of the limitations of this ultra-fast technique is assuming that slowed or halted DNA replication after 15 min antibiotic exposure indicates susceptibility of a bacterial population to a given antibiotic. However, the bacterial population response within the first 15 min is typically highly variable among assay replicates, which can increase the error in the prediction of susceptibility,[17] especially when borderline MIC concentrations of antibiotics are tested.

Change of bacterial viability in response to antibiotics can also be measured by probing bacterial shape,[18] motion,[19] size/mass,[20,21] or respiration/redox state.[22,23] Among them, AST methods which rely on monitoring bacterial motion have been extensively explored. Johnson et al. used the phase noise of a resonant crystal to show that the motion of *E. coli* was attenuated after treatment with polymyxin B or ampicillin (AMP).[24] This work demonstrates bacterial motion as a promising characteristic for RAST. Yu et al. reported a phenotypic AST that utilized deep learning to analyze freely moving *E. coli* cells in urine to determine the MIC in 30 min.[18] In another RAST method developed by Resistell Co., change of bacterial viability is measured using a resonating cantilever (as used in atomic force microscopy) which is sensitive to bacterial movement.[25] However, these methods have poor sensitivity and/or require labeling[26] or indicative markers such as redox-active chemicals, which can interfere with cellular physiology.[23] In addition, some of these methods still need advanced imaging/analysis setups, such as high-resolution optical microscopy, atomic force microscopy, or complex optical setups,[18,27] which limit their broad applicability in clinical diagnostics.

Compared to optical methods that visually assess changes in the shape, length, and/or motion of bacterial cells, measuring the light attenuation scattered off bacterial populations is a simpler method that eliminates the need for a bulky and high-cost optical setup. One of such methods is laser scattering, which has been utilized in developing RAST. For example, the BacterioScan system (BacterioScan Inc.) measures the optical density (OD) of a liquid sample as well as the low-angle laser scattered intensity which enables measurements of significantly lower OD levels compared to traditional ratiometric transmittance measurements.[28] However, this method is based solely on OD, which does not provide substantial improvement of the RAST turnaround time (∼6 h).

To further reduce the detection time, we propose dynamic laser speckle imaging to quantify bacterial micromotion and correlate the decrease of micromotions with the inhibitory effects of antibiotics. The method is based on the phenomenon of laser light scattering in scattering media, such as biological tissues.[29] The self-interference of the scattered light produces a speckle pattern that conveys characteristics of the scatterers and the nature of their dynamic behavior over time. When the light is scattered from a static turbid medium, a constant laser speckle pattern is generated due to the fixed phase relationship.[30−33] On the contrary, if scatterers in the medium exhibit movement, the scattering pattern will evolve over time, generating a dynamic speckle pattern.[34] A time series of dynamic speckle images contains information about particles' kinetic behavior and can be used as a means to probe the effect of environmental triggers, including antibiotics, on their motion. For example, Murialdo et al. used dynamic laser speckle imaging (DLSI) to detect different degrees of motility and chemotaxis in bacteria-swarming plates.[31] Ramírez-Miquet et al. proposed a technique combining speckle imaging with a digital image information technology to track multiplying *E. coli* and *Staphylococcus aureus* cells deposited on agar plates at high concentrations of 1.5×10^9 and 10^9 cells/mL, respectively.[34] They compared the mean viability of each pathogen and showed that this speckle imaging method has the potential to detect biological activity in 15 min.

Despite these efforts, to the best of our knowledge, there is no report of an application of time-resolved DLSI for antibacterial susceptibility testing in liquid samples. Moreover, previously reported assays are not sensitive enough for rapid analysis of cells at 5×10^5 cells/mL, a concentration required by the gold standard protocols. We show that analysis of time-resolved DLSI data using an artificial neural network (ANN) can identify the MIC of AMP and gentamicin (GEN) for *E. coli* K-12 in 60 min with high accuracy compared to gold standard methods using a voting strategy for the ANN predictions. In addition to AMP and GEN, our method can determine MIC of ceftriaxone accurately. Additional tests were conducted on a multidrug-resistant (MDR) strain of *E. coli* and a clinical isolate of *S. aureus*. The results were validated using the gold standard BMD and time-kill curves. In our machine learning model, we adapted a multilayer perceptron (MLP) for classification and prediction. MLP can in principle approximate any measurable function to any desired degree of accuracy with its capability to set highly nonlinear boundaries between classes[35] and has been proven as a superior algorithm for many applications, such as malware detection system and lung cancer classification.[36] The developed dynamic laser imaging-based RAST method (DyRAST) is fast, label-free, and eliminates the need for advanced microscopy systems. Compared with the method of dynamic light scattering (DLS),[37] which is commonly used to characterize nanoparticles, DLSI can simultaneously capture a time series of laser scattering patterns over a range of angles (limited by the field of view of the image sensor). The large amount of evolving spatiotemporal data lend to the use of advanced data analytics (such as machine learning in this work), which is applicable to both single scattering or multiple scattering regimes and can thus enable analysis of both highly diluted and highly concentrated samples. In addition, development of DyRAST involves simple

https://dx.doi.org/10.1021/acssensors.0c01238
ACS Sens. 2020, 5, 3140−3149

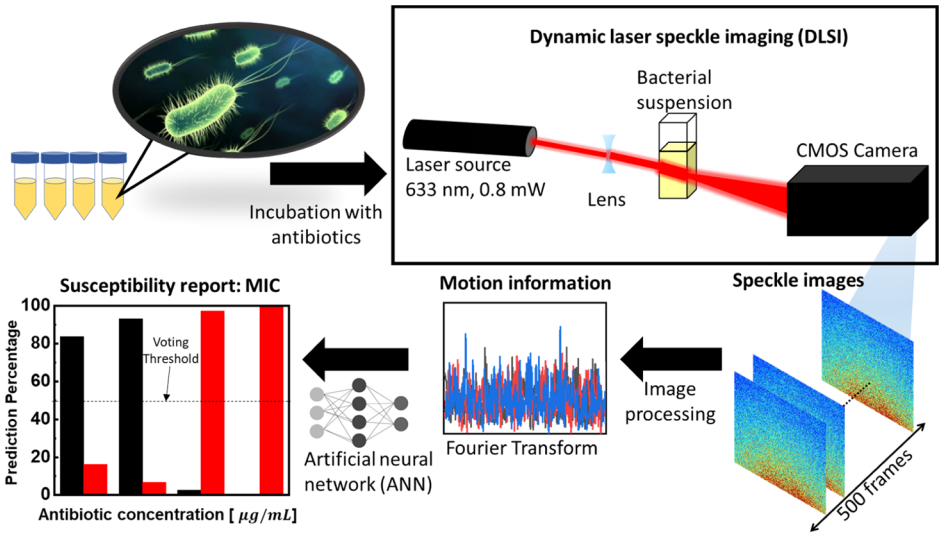

Figure 1. Schematic of the dynamic speckle imaging setup for RAST (DyRAST). After expansion by the lens, the laser beam is scattered by the bacterial culture in the cuvette containing different concentrations of antibiotic (ρ_{Antb}). At each time point (t_i), the dynamic speckle patterns are recorded, for total time of 10 s, 500 frames. After preprocessing, Fourier analysis reveals the information characterizing bacterial motion. The Fourier results are then fed into an ANN for prediction of MIC.

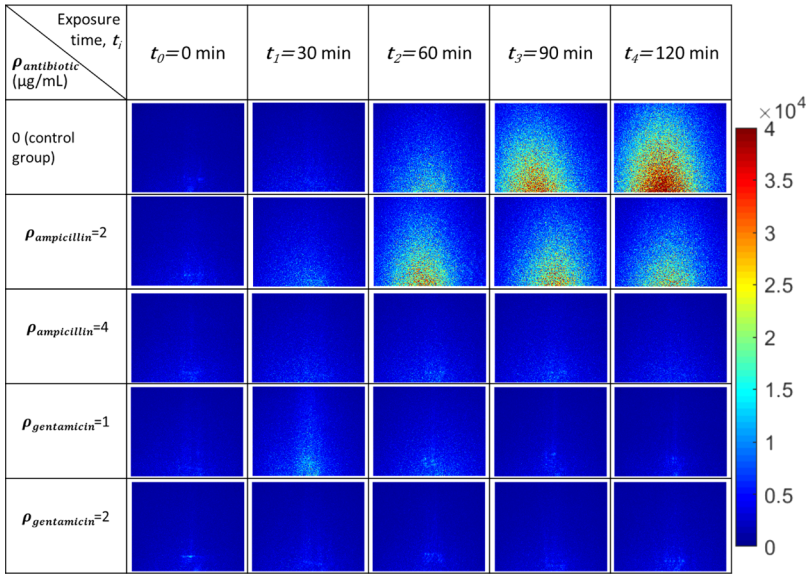

Figure 2. Raw speckle images. The speckle images of *E. coli* K-12 exposed to AMP and GNT at different concentrations (ρ). MIC of AMP and GEN was 4 and 2 μg/mL, respectively. The images were collected over a total period of 2 h with 30 min intervals at time points, t_i (i = 0, 1, ..., 5). The images were collected using the optimized setup (setting #3).

optics and electronics (with potential to incorporate consumer electronics such as cellphone cameras), which can significantly improve the accessibility of the phenotypic RAST.

RESULTS AND DISCUSSION

Figure 1 shows a schematic of the DLSI setup consisting of a laser source, lens, cuvette holder, and camera. Distances between the setup components are listed in the Supporting Information, Table S1. The optical image of the setup is shown in the Supporting Information, Figure S1. We have optimized the setup (in terms of the distance between different components and the scattered light angle, θ) guided by the Mie scattering model described in the Supporting Information, Section S2. We investigated three configurations: setting #1−3. An important parameter in the setup is the angle between the axis of the camera and the laser beam (θ). The setup with setting #3 (with $\theta \sim 15°$) enables high-sensitivity DLSI measurements, consistent with the Mie scattering theory (Figure S5, Supporting Information) while preventing the direct incidence of the laser beam on the camera which can saturate the image sensor. The results reported in the rest of the paper are based on this configuration, unless otherwise stated.

Figure 2 shows typical speckle patterns of *E. coli* K-12 culture captured at t_i = 0, 30, 60, 90, and 120 min with different concentrations of AMP and GEN (ρ_{AMP} and ρ_{GNT}), with respective MIC values of 4 and 2 μg/mL (confirmed using gold standard methods; see the Materials and Methods section). The speckle patterns for the control experiment (without antibiotics) are shown in the first row. In the absence

https://dx.doi.org/10.1021/acssensors.0c01238
ACS Sens. 2020, 5, 3140−3149

of antibiotics, bacterial cells multiply. Their multiplication and division translate into an increase in the total number of scatterers and hence an increase of the intensity of the speckle patterns over time. At sub-inhibitory MIC concentration (e.g., 0.5 × MIC value shown in the second and fourth rows, for AMP and GNT, respectively), there is an initial increase of the speckle intensity, followed by a slight decrease at 120 min. When cells are exposed to MIC (the third and fifth rows, for AMP and GEN, respectively), there is no significant change in the speckle intensity over time, which indicates inhibition of bacterial division.

The OD data and the average intensity values obtained from raw speckle patterns (examples shown in Figure 2) are shown in Figure 3A–D for AMP and GEN, respectively. The average

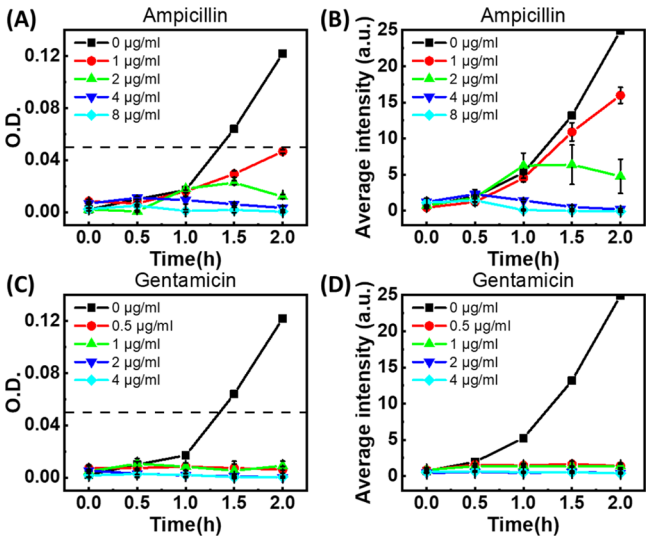

Figure 3. Turbidity data (OD measurement) and average intensity of raw speckle images. (A) OD_{600} values vs treatment time and (B) average intensity results obtained from raw dynamic laser speckle images of *E. coli* K-12 with AMP with ρ_{AMP} = 0, 1, 2, 4, and 8 μg/mL. (C) OD_{600} values vs treatment time and (D) average intensity results obtained from raw dynamic laser speckle images of *E. coli* K-12 with ρ_{GNT} = 0, 0.5, 1, 2, and 4 μg/mL. The dashed lines in panels (A,C) indicate the detection limit of the commercial OD measurement system. The MICs for AMP and GEN were 4 and 2 μg/mL, respectively, as determined by the gold standard method (results shown in Figures 5A and 6A).

intensity for raw pixelated speckle images was calculated for each image matrix collected at t_is [hence, obtaining a data cube of 1000 × 2000 (pixels) × 500 (# of frames)]. It is worth mentioning that the average DLSI intensity captures time-kinetics of *E. coli* growth and is more sensitive than conventional OD measurements (with detection limit indicated by dashed lines in Figure 3). While the OD values for different antibiotic concentrations are below the detection limit of the OD reading even after 120 min, the average speckle intensity values are distinguishable in 90 min.

However, simple intensity measurements are "blind" to the overnight (>16 h) turbidity/colony count results (Figures 3A/5A and 3C/6A for AMP and GEN, respectively) and prone to false prediction; for example, intensity data determines AMP MIC as 2 μg/mL (Figure 3), while the correct MIC based on the overnight data is 4 μg/mL (Figure 5A). The intensity measurement also neglects the time-resolved motion information of cells. Moreover, absolute intensity is heavily influenced by the specifics of the optical setup (laser power, exposure time, camera gain, etc.). This presents a challenge to calibrate and extend the methodology to a generalized case. To overcome this problem, we utilize machine learning and train ANN models using the gold-standard overnight results to analyze the dynamic speckle patterns and determine MIC. Figure 4 illustrates our methodology for preprocessing the data and applying the machine learning algorithm. As shown in Figure 4A, Fourier transform (FT) analysis was performed along the time axis on individual pixels, with the DC component (direct current component which is the value at 0 Hz) normalized to 1 (details provided in the Supporting Information, Section S3) to ensure that the analysis is independent of the absolute speckle intensity values. For each time point, t_i, of each group, we obtained 20,000 pixel-level spectra, each consisting of 249 frequency features. We then built a separate ANN model for each time point with 249 neurons at the input, 300 hidden units, and 2 output neurons for binary classification.

We trained the ANN models with experimental data for *E. coli* K-12 exposed to antibiotics of different concentrations (0.25×, 0.5×, 1×, and 2 × MIC). We conducted experiments in three independent replicates with groups exposed to four concentrations for each antibiotic. The four concentrations yielded a total of 80,000 spectra for each time point. As shown schematically in Figure 4B, we split the samples randomly into training, validation, and test groups with ratios of 70, 15, and 15%, respectively. The validation was performed to avoid model overfitting, and the test group was used to verify the predictive power of the trained neural networks. Two independent experiments, with each experiment utilizing four different concentrations of the antibiotic which result in a combined data size of 160,000 samples at each time point, were used in building the learning models. We then used a third, independent experiment that consisted of 80,000 spectra at each time point for a final comprehensive test to evaluate the robustness and accuracy of the trained models.

The overnight OD values were utilized to label the dataset. If the OD after overnight incubation was at the same level as the initial OD, the bacterial group was labeled as "inhibited". On the other hand, if the final OD was higher than the initial OD value (above the resolution limit of the equipment which is ~0.05), the group was labeled as "non-inhibited". In our experiments, 0.25× and 0.5 × MIC were labeled as "non-inhibited", while 1× and 2 × MIC were labeled as "inhibited". For each group at time point t_i, the result of the test is interpreted using a voting process where the percentage of each prediction category indicates the likelihood for this group to be classified as the said category. For example, 30% "inhibited" implies 30% of the 20,000 spectra are predicted "inhibited", while the remaining 70% are predicted to be "non-inhibited". Therefore, this group would be classified as "non-inhibited". As shown in Figure 4C, we also evaluated the effect of the resizing factor on the performance (prediction percentage) of the machine learning analysis. The black bar indicates the percentage of pixels "non-inhibited", while the red bar indicates the percentage of "inhibited". With 100 × 200, 25 × 50, and 10 × 20 resizing factors, we observed only a 5% difference among the machine learning results. Furthermore, they all correctly predict MIC in 60 min through the voting strategy using a 50% threshold for decision-making. The ability to reduce the data size using a higher resizing factor indicates that the required computational resources can be reduced

https://dx.doi.org/10.1021/acssensors.0c01238
ACS Sens. 2020, 5, 3140−3149

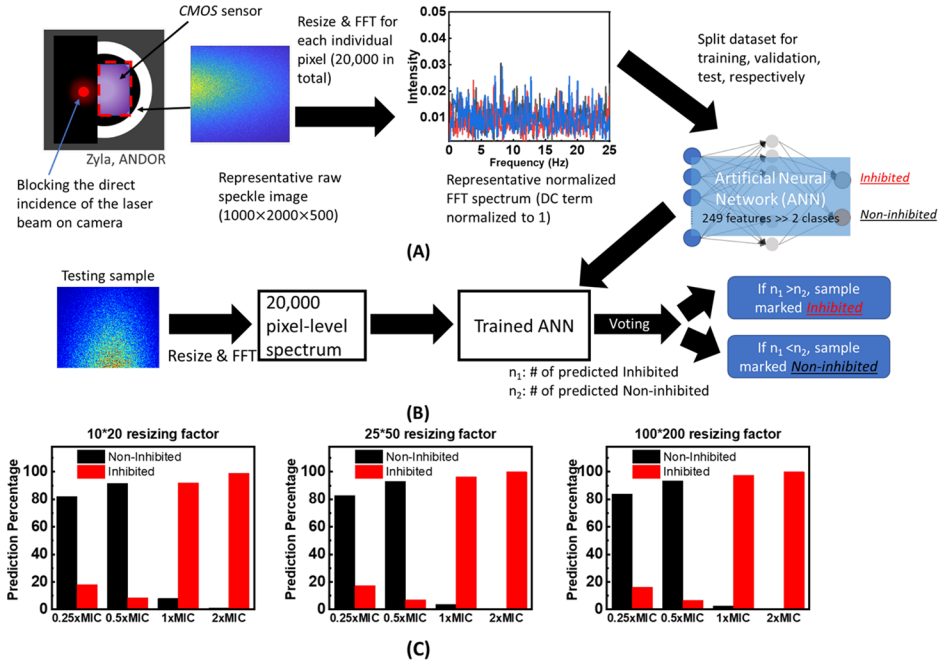

Figure 4. Analysis of DLSI data using machine learning enables rapid AST. (A) Raw speckle images were collected at each t_i. The incident laser beam was blocked to ensure that it does not directly hit the camera to avoid saturation. The time series at each pixel was Fourier transformed with the DC term normalized to 1. Fourier results, i.e., the resultant features, were fed into the ANN model with 249 neurons as the input, 300 hidden units, and 2 output neurons for binary classification. (B) Trained ANN model was tested using a separate set of data. Similarly, 20,000 pixel-level spectra were preprocessed and fed into the trained ANN. Through voting (threshold at 50%), we determined the susceptibility of the bacterial sample ("inhibited" vs "non-inhibited"). (C) Comparison of the ANN algorithm with different resizing factors. Prediction percentage of ANN with 100 × 200, 25 × 50 or 10 × 20 resizing factor is almost identical (within 5% difference).

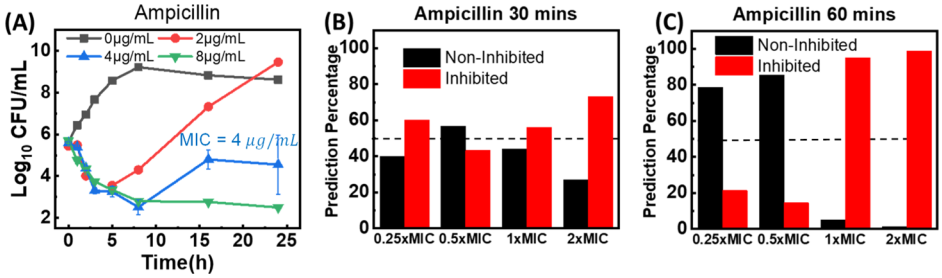

Figure 5. Voting strategy enables accurate and rapid prediction of AMP's MIC. (A) Time-kill curves for *E. coli* K-12 with different concentrations of AMP. The prediction percentage of machine learning algorithm improves with time: (B) results using DLSI data collected at t_2 = 30 min and (C) results using DLSI data collected at t_3 = 60 min. After 60 min, the method can identify MIC with high accuracy. The dashed lines indicate the voting threshold (50%) to predict AST results with high accuracy, i.e., "inhibited" for 1 × MIC and 2 × MIC, while at the same time "non-inhibited" for 0.25 × MIC and 0.5 × MIC. AMP MIC was 4 μg/mL.

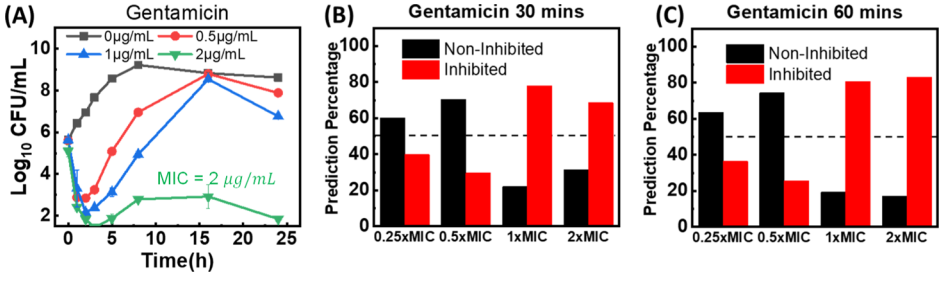

Figure 6. Voting strategy enables accurate and rapid prediction of GEN's MIC. (A) Time-kill curves for *E. coli* K-12 with different concentrations of GEN. The prediction percentage of machine learning algorithm improves with time: (B) results using DLSI data collected at t_2 = 30 min and (C) results using DLSI data collected at t_3 = 60 min. The dashed lines indicate the voting threshold (50%) to predict AST results with high accuracy, i.e., "inhibited" for 1 × MIC and 2 × MIC, while at the same time "non-inhibited" for 0.25 × MIC and 0.5 × MIC. GEN MIC was 2 μg/mL.

https://dx.doi.org/10.1021/acssensors.0c01238
ACS Sens. 2020, 5, 3140−3149

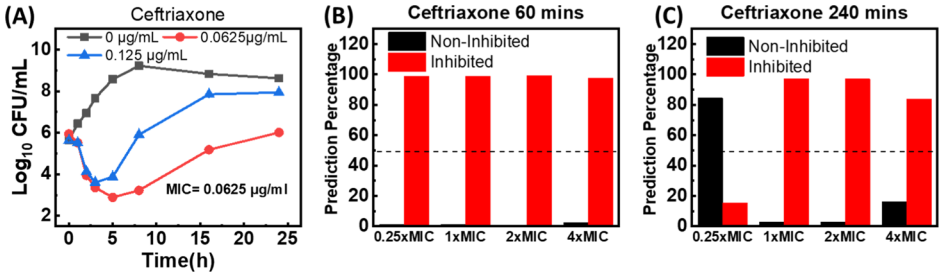

Figure 7. Voting strategy enables accurate and rapid prediction of ceftriaxone's MIC. (A) Time-kill curves for *E. coli* K-12 with different concentrations of ceftriaxone. The prediction percentage of machine learning algorithm improves with time: (B) results using DLSI data collected at t_1 = 60 min and (C) results using DLSI data collected at t_4 = 240 min. The method can predict MIC for ceftriaxone in 240 min. The dashed lines indicate the voting threshold (50%) to predict AST results with high accuracy, i.e., "inhibited" for 1 × MIC, 2 × MIC, and 4 × MIC, while at the same time "non-inhibited" for 0.25 × MIC. Ceftriaxone MIC was 0.0625 μg/mL.

without significant performance degradation. It should be noted that the machine learning method does not rely on the absolute speckle intensity which could be difficult to calibrate. Detailed discussion on machine learning and confusion matrices (which allow visualization of the ANN performance) are provided in the Supporting Information, Section S4.

The machine learning results for the prediction of AMP and GEN susceptibility and their MIC values are shown in Figures 5 and 6, respectively. Figures 5A and 6B show the time-kill curves obtained using the broth macrodilution method. The MIC was defined as the minimal concentration at which bacterial population remained at or below the level of initial inoculum concentration. Hence, if at a given antibiotic concentration the culturable bacterial population substantially decreased in initial hours but later on resumed growth and surpassed the initial inoculum concentration, that antibiotic concentration was considered sub-inhibitory. The pixel-level prediction percentage obtained using machine learning is shown in Figures 5B,C and 6B,C, for AMP and GEN, respectively. Figure 5B suggests that 30 min is not long enough for accurate prediction of MIC. We defined the final classification result based on the voting strategy described above: the dashed lines in Figures 5 and 6 indicate the voting threshold to predict antimicrobial susceptibility. A correct prediction means classification as "inhibited" for 1 × MIC and 2 × MIC, while at the same time, 0.25 × MIC and 0.5 × MIC should be classified as "non-inhibited". For example, at 30 min, the predicted percentage of classification as "inhibited" for 2 × MIC of AMP is ∼50%, making it difficult to decide in which class/label the sample belongs to. While at 60 min, the correct classification ("inhibited") is predicted in more than 80% of the votes. Interestingly, by comparing Figures 5 and 6, it is observed that the method can predict MIC for GEN in 30 min (compared to 60 min for AMP). Hence, for accurate analysis of DLSI data and identifying MIC, DyRAST required a minimum of 60 min in our studies with AMP and GEN. The pixel-level prediction percentage difference increased with time, as shown in the Supporting Information, Figures S10 and S11 for AMP and GEN, respectively.

It is worth noting that by counting viable cells using the broth macrodilution technique (a sensitive yet slow and laborious method), differentiation among 0.5 × MIC, 1 × MIC, and 2 × MIC was possible only after 5 h for AMP and after 2 h for GEN (see Figures 5A and 6A) in our studies. The only alternative rapid phenotype-based method available on the market and approved by the FDA requires at least 6 h culture incubation to confidently determine the antimicrobial susceptibility.[15] It should be noted that the difference between speckle imaging results and the time-kill results (initially seeming inhibitory for sub-MIC concentrations) could be due to viable but non-culturable cells (VBNC). VBNCs are live and active when the speckle images are captured but cannot grow to a detectable level on an agar plate.[38] Yet, DyRAST can accurately determine the MIC of AMP and GEN for *E. coli* K-12 within 1 h of culturing an isolate (despite the initial seemingly inhibitory effect of sub-MIC concentration). This is a distinct feature of our system to determine the MIC correctly despite the potential gradual adaptation of bacteria to antibiotics, which may lead to a false diagnosis if overlooked.

We also studied the performance of DyRAST for determining MIC of ceftriaxone (a third-generation cephalosporin)[39] on *E. coli* K-12. OD_{600} curves, raw speckle images, and average speckle intensity values for control cultures and cultures treated with MIC (determined using BMD method) are provided in the Supporting Information, Figure S12. Figure 7A plots the time-kill curves for control, MIC, and 2 × MIC of ceftriaxone. Figure 7B,C depict the prediction percentage results at 60 min and 4 h obtained using the ANN model, suggesting that at least 4 h is needed to determine MIC of ceftriaxone. Figure S13 in the Supporting Information summarizes the ANN prediction percentage results for other time points, indicating that accuracy increases with time, similar to the previous cases with AMP and GEN.

In order to further demonstrate applicability of the DLSI system for monitoring bacterial viability beyond *E. coli* K-12, we performed preliminary experiments with a MDR *E. coli* (treated with AMP and GEN) and a clinical isolate of *S. aureus* treated with AMP. Time-kill curves for these strains are plotted in the Supporting Information, Figure S14. OD_{600} curves, raw speckle images, and average speckle intensity values are provided in the Supporting Information, Figure S15 (for MDR *E. coli* treated with AMP), Figure S16 (for MDR *E. coli* treated with GEN), and Figure S17 (for *S. aureus* treated with AMP). For MDR *E. coli*, we also tested a concentration of AMP and GEN that serves as a clinical resistance diagnosis breakpoint (intermediate breakpoint concentration: 16 μg/mL for AMP and 8 μg/mL for GEN) determined by the Clinical and Laboratory Standards Institute (CLSI) guideline (M100 ED30:2020). Figure S18A−C depicts the time-evolution of the Fourier component at 10 Hz for MDR *E. coli* treated with AMP and GEN (breakpoint concentration and MIC) and *S. aureus* treated with AMP (control and MIC), respectively. A larger FT component indicates more dynamic scattering, and hence a higher rate of change (e.g., because of bacterial

https://dx.doi.org/10.1021/acssensors.0c01238
ACS Sens. 2020, 5, 3140−3149

Table 1. Comparison of This Work with Some of the Recent Size/Motion-Based RAST Methods

method	cell concentration	sample	AST time	validation method	setup complexity	refs
Accelerate PhenoTest BC Kit	10^5 cell/mL	clinical specimens	6 h	compared with disk diffusion result	high (require labeling)	15
oCelloScope	2×10^7 cell/mL	veterinary samples	3 h	N/A	low	41
Drast	5×10^5 to 5×10^7 cell/mL	bacteria added to fresh blood	6 h	compared with BMD	high (microscopy)	42
SNDA−AST	5×10^5 cell/mL	clinical isolates and urine samples	<5.5 h	N/A	high (microscopy)	1
stress-based microfluidic system	100−4000 cells in 12 nL	four Gram-negative strains in MHB	<1 h	MIC determined using VITEK	high (microscopy)	43
laser ablation electrospray ionization mass spectrometry	1.5−2.5 cells per 1000 μm^2	disk	21 h	compared with MIC database	high (microscopy)	44
nanomotion sensor	OD = 0.5	clinical *Bordetella Pertussis*	3 h	compared with BMD	high (AFM[b] setup)	45
nanomotion-AST	100 cell/mL	bacteria in human blood	<3 h	N/A	high (AFM setup)	46
Astrego Captiver	10^4 cell/mL	urine sample	30 min	N/A	high (microscopy)	16
Q-linea ASTar	5×10^5 cell/mL		6 h	compared with BMD	high	47
QuickMIC	1:50 dilution of 0.5 McFarland	clinical isolates	4 h		high (microscopy)	48
surface area assay	5×10^5 cell/mL	bacteria in MHB[a]	5 h	compared with BMD	high (microscopy)	49
BacterioScan	10^5 cell/mL	bacteria in MHB	6 h	N/A	low	28 and 50
DyRAST	5×10^5 cell/mL	bacteria in MHB	1 h	compared with BMD	low	this work

[a]MHB: Mueller-Hinton broth. [b]AFM: atomic force microscopy.

movement). These results suggest that laser speckle imaging, when combined with machine learning, is able to differentiate between viability under inhibitory and non-inhibitory conditions (in 1 h for *S. aureus* and MDR *E. coli* and in 4 h for ceftriaxone). For MDR *E. coli*, our method enabled identification of the resistance against AMP and GEN in 1 h (based on the data for the breakpoint concentrations).

Table 1 compares the performance of DyRAST reported in this study with other size/motion RASTs based on the initial cell concentration, RAST time, sample condition, and setup complexity. In contrast with methods based on microfluidics or other methods (e.g., based on atomic force microscopy), DyRAST does not require expensive instrumentation and utilizes similar tools as the existing AST assays which are already formulated, verified, and validated and are widely available at a relatively low cost. Therefore, the proof-of-concept method presented here may offer a promising route for developing a portable, affordable, and automated RAST for application in resource-limited areas, which is critical in our global fight for the AMR stewardship. Toward this goal and to translate the proof-of-principle studies in this work to clinical settings, a detailed analysis using a library of various clinical strains and different antibiotics is required. Moreover, future extension of this work includes study of more complex media (such as urine) and optimization of the DyRAST system to enable analysis of lower initial bacterial concentration (e.g. 1000 CFU/mL) without sacrificing the assay time.

CONCLUSIONS

This work presents a rapid, phenotype-based antibacterial susceptibility testing method. The method leverages machine learning analysis of time-resolved DLSI patterns to predict antimicrobial susceptibility based on the change in bacterial motion in response to antibiotics and determine MIC in a rapid and reliable manner. The DLSI data was collected using a simple-to-use, low-cost optical setup with no labeling or advanced imaging/optical setup required. To demonstrate the capabilities of the method (termed as DyRAST), we studied the effects of AMP, GEN, and ceftriaxone on *E. coli* K-12 and achieved MIC prediction in 60 min for the first two, and 4 h for ceftriaxone. DyRAST was validated against the gold standard AST method (BMDs). By adapting a voting strategy for analysis of the pixel-level prediction values obtained using an ANN model, the method predicted MIC with high accuracy comparable with BMD, but much faster, in all tested conditions. The technique can be optimized for analysis of other (pathogenic) bacterial and fungal species and their response to antimicrobial treatment. Moreover, considering no complicated optical components are required for speckle imaging, a portable version of DyRAST can potentially be developed using consumer-level components. Further work based on this proof of concept is needed to evaluate the method's performance on a broader panel of microorganisms and antibiotics.

MATERIALS AND METHODS

Bacterial Culture. *E. coli* strain K-12 was used as a model bacterial strain in all experiments with ampicillin, gentamicin, and ceftriaxone. MDR *E. coli* strain PS00278A (porcine isolate) was tested with ampicillin and gentamicin to contrast with the susceptible model bacterial strain. *S. aureus* strain PS00975A (human clinical isolate) was used with ampicillin to evaluate the methods' performance on a Gram-positive microorganism. Cultures were stored as frozen stocks at −80 °C and resuscitated every 14 days to maintain a fresh inoculum. The culture was resuscitated by streaking onto Mueller Hinton agar (MHA) and was then incubated at 37 °C for 20 ± 2 h. A single colony from the MHA agar was re-streaked on a fresh MHA plate and incubated at 37 °C for 20 ± 2 h. A single colony from the MHA sub-streak plate was inoculated into 10 mL of Mueller Hinton broth (MHB) and incubated at 37 °C, shaking at 210 rpm, for 20 ± 2

https://dx.doi.org/10.1021/acssensors.0c01238
ACS Sens. 2020, 5, 3140−3149

h. The overnight culture was diluted in MHB based on the OD_{600} to obtain 5×10^5 CFU/mL using a BioPhotometer D30 (Eppendorf, Hauppauge, NY). An OD_{600} of 1 was considered to be equal to 8×10^8 CFU/mL, based on an *E. coli* OD_{600}—CFU/mL standard curve.

Preparation of the Antibiotics. Ampicillin (Sigma-Aldrich, CAS# 7177-48-2), gentamicin (Sigma-Aldrich, CAS# 1405-41-0), and ceftriaxone (Sigma-Aldrich, CAS# 104376-79-6) stock solutions were prepared by dissolving antibiotic powder in sterilized Milli-Q ultrapure water to achieve 5 and 10 mg/mL stock solutions, respectively. All stock solutions were frozen in 0.1 mL aliquots and stored at −20 °C.

Antimicrobial Susceptibility Testing Using Broth Microdilution. The 5×10^5 CFU/mL culture was used for BMD and speckle imaging. For BMD, the standard methods recommended by the CLSI guideline M100-S22[40] was applied to determine the MIC of the studied antibiotics for *E. coli* strain K-12, MDR *E. coli* strain PS00278A, and *S. aureus* strain PS00975A. The CLSI guideline M100 ED30:2020 was used to define clinical resistance based on determined MICs. For both methods, 50 μL of MHB was aliquoted in wells of 96-well microtiter plates (Greiner Bio-One). Antibiotics were added to the wells of the first row and sequentially diluted two-fold down the row. 50 μL of culture prepared as described above was added to each well and incubated for 16−20 h. Negative and positive controls were included in each test plate, and each test was carried out in three biological replicates per independent experiment and at least two independent experiments. MIC was determined by visually inspecting wells for turbidity resulting from culture growth.

Verifying Antimicrobial Susceptibility Using Time-Kill Kinetics. Broth macrodilution was used to determine the time-kill kinetics with all strains; culture in concentration of 5×10^5 CFU/mL was first grown for 1 h at 37 °C in a shaking condition (210 rpm) and was then exposed to different antibiotics with various concentrations, as indicated. Viable cells were quantified at times 0, 1, 2, 3, 5, 8, 16, and 24 h by spiral plating (easySpiral, Interscience) 10-fold dilutions onto MHB agar. Inoculated plates were incubated at 37 °C for 16−20 h and counted to determine the CFU/mL at each time point. All experiments were completed using three biological replicates and three technical replicates per plate.

DLSI Setup. A helium−neon laser (wavelength: 632.8 nm, power: 0.8 mW, HNLS008L, Thorlabs Inc., USA) was used as the illumination source. The laser beam was slightly expanded by using a concave lens (focal length = −25.0 mm) before illuminating a cuvette (Fisherbrand, CAS# 14-955-129) containing 3 mL of bacterial suspension. The resultant speckle pattern was captured by a CMOS camera (Zyla, Andor) interfaced to a computer. Note that other methods, such as an inverse telescope beam expander, can also be used to increase the incident laser beam size. Our choice of a diverging lens is due to its simplicity and compactness as well as the fact that an explicit physical model is not needed for the machine learning-based analysis, which relaxes the requirement of a plane-wave incident beam as commonly used in dynamic light scattering. In addition, the diverging angle is small enough (∼1°) so that Mie scattering analysis (that assumes a planar incident wave and spherical scatterers) can still be used to estimate the scattering phase function in order to guide the optimization of the experimental setup, which, in this work, is configured to collect light scattering within an angular range of between 11 and 22°. This optimization is particularly important for increasing the sensitivity for measuring low-concentration samples which produce weak speckle patterns.

Antibacterial Susceptibility Testing Using DLSI. For DLSI-based AST, the culture grown as outlined above was adjusted to 5×10^5 CFU/mL and was further incubated at 37 °C, 210 rpm for 1 h to reach the logarithmic growth phase before an antibiotic was added to the culture in concentrations equal to 0 × MIC (control), 0.25 × MIC, 0.5 × MIC, 1 × MIC, and 2 × MIC. Three milliliter of each culture was collected at each time point, t_i (i = 0, 1, ..., 4) at 0, 30, 60, 90, and 120 min, respectively, and transferred into the cuvette used for DLSI in the imaging system described above. At each t_i, a dynamic speckle patterns series (16 bits, 1000 × 2000 pixels, 50 frames per s) was collected. The exposure time for each frame was 1 ms, and the full capture period was 10 s at each time point, t_i. All experiments were conducted in independent triplicates.

Image Preprocessing and Machine Learning Model. The raw images (1000 × 2000) were first resized (100 × 200) using the nearest-neighbor method to reduce the computational cost. The camera had a pixel size of 6.5 μm, corresponding to a 6.5 mm × 13 mm detection area. Fourier transform (FT) was performed along the time axis of the measured data cube. Only the spectral intensity was utilized in our analysis since a spectral intensity distribution with significant high-frequency content generally corresponds to more active motion, while the spectral phase is not directly linked to motion activeness and presents a challenge in quantitative interpretation. This procedure transformed an original 100 × 200 × 500 data cube (two-dimensional space and one-dimensional time) into a new 100 × 200 × 249 data cube consisting of 249 positive frequency sampling points at each pixel position. The DC term was first normalized to 1 for each individual pixel spectrum and was subsequently removed. The negative frequencies provided identical information as their positive counterparts. Each measurement captured 20,000 spectra, and each of the spectra contained 249 frequency features. This large data set was necessary for machine learning-based analytics.

The experimental replicates were pooled, processed together, and then divided randomly into training, validation, and test groups. An ANN with a hidden layer containing 300 neurons was constructed for classification prediction. The input layer contained 249 neurons, representing the frequency components, up to 25 Hz. The output was separated into 2 classes, "inhibited" and "non-inhibited", referring to either bacterial susceptibility or antibiotic resistance. The stochastic gradient descent method was used to minimize the binary cross-entropy loss function. Binary classification for the "inhibited" and "non-inhibited" bacteria groups was determined with the input from the frequency domain for each pixel. All image preprocessing and machine learning computations were performed with a desktop computer (Intel Core i9-9900k, 32 GB RAM, NVIDIA RTX 2080 Ti). The training takes ∼2 min, and the FT analysis for one entire independent experiment takes ∼5 min.

■ ASSOCIATED CONTENT

Supporting Information

The Supporting Information is available free of charge at https://pubs.acs.org/doi/10.1021/acssensors.0c01238.

Optical setup; raw speckle images with setup 1−3; Mie scattering analysis for setup optimization; FT analysis; machine learning prediction results for *E. coli* K-12 with AMP and GEN; results with MDR *E. coli*, *S. aureus*, and ceftriaxone; optical components configuration; and confusion matrix for the ANN model and time-evolution (PDF)

■ AUTHOR INFORMATION

Corresponding Authors

Zhiwen Liu − *School of Electrical Engineering and Computer Science and Materials Research Institute, The Pennsylvania State University, University Park, Pennsylvania 16802, United States*; Phone: 814-865-2362; Email: zzl1@psu.edu

Aida Ebrahimi − *School of Electrical Engineering and Computer Science, Materials Research Institute, and Department of Biomedical Engineering, The Pennsylvania State University, University Park, Pennsylvania 16802, United States*; orcid.org/0000-0002-4013-7816; Phone: 814-865-6177; Email: sue66@psu.edu

Authors

Keren Zhou − *School of Electrical Engineering and Computer Science and Materials Research Institute, The Pennsylvania*

https://dx.doi.org/10.1021/acssensors.0c01238
ACS Sens. 2020, 5, 3140−3149

State University, University Park, Pennsylvania 16802, United States

Chen Zhou − *School of Electrical Engineering and Computer Science and Materials Research Institute, The Pennsylvania State University, University Park, Pennsylvania 16802, United States*

Anjali Sapre − *Department of Food Science, The Pennsylvania State University, University Park, Pennsylvania 16802, United States*

Jared Henry Pavlock − *Department of Food Science, The Pennsylvania State University, University Park, Pennsylvania 16802, United States*

Ashley Weaver − *Department of Food Science, The Pennsylvania State University, University Park, Pennsylvania 16802, United States*

Ritvik Muralidharan − *School of Electrical Engineering and Computer Science, The Pennsylvania State University, University Park, Pennsylvania 16802, United States*

Josh Noble − *School of Electrical Engineering and Computer Science and Materials Research Institute, The Pennsylvania State University, University Park, Pennsylvania 16802, United States*

Taejung Chung − *Department of Food Science, The Pennsylvania State University, University Park, Pennsylvania 16802, United States*

Jasna Kovac − *Department of Food Science, The Pennsylvania State University, University Park, Pennsylvania 16802, United States*

Complete contact information is available at: https://pubs.acs.org/10.1021/acssensors.0c01238

Author Contributions

K.Z. and C.Z. contributed equally to this work. K.Z. wrote the manuscript, designed and optimized the optical setup, performed antibacterial susceptibility testing using DLSI, and analyzed the data. C.Z. wrote the manuscript, designed and optimized the optical setup, developed the ANN algorithm, and analyzed the data. A.S., J.H.P., A.W., and T.C. performed the MIC determination and time-kill experiments. R.M. and J.N. assisted with the optical setup. J.K. guided the microbiology experiments and reviewed the manuscript. A.E. and Z.L. designed and supervised the research, wrote the manuscript, and analyzed the data.

Notes

The authors declare no competing financial interest.

■ ACKNOWLEDGMENTS

This work was supported through the Materials-Life Science Convergence Award provided by the Materials Research Institute, Huck Institutes of Life Sciences, College of Engineering, and College of Medicine (Hershey) at Penn State. Z.L. and C.Z. acknowledge the support by Penn State MRSEC, Center for Nanoscale Science, under the award NSF DMR-1420620. J.K. was partially supported by the USDA National Institute of Food and Agriculture Hatch Appropriations under project #PEN04646 and accession #1015787. We thank Dr. David Craft (the Director of Clinical Microbiology at Hershey Medical Center) for providing the clinical *S. aureus* strain used in this study.

■ REFERENCES

(1) Avesar, J.; Rosenfeld, D.; Truman-Rosentsvit, M.; Ben-Arye, T.; Geffen, Y.; Bercovici, M.; Levenberg, S. Rapid Phenotypic Antimicrobial Susceptibility Testing Using Nanoliter Arrays. *Proc. Natl. Acad. Sci. U.S.A.* **2017**, *114*, E5787−E5795.

(2) Willyard, C. The Drug-Resistant Bacteria That Pose the Greatest Health Threats. *Nature* **2017**, *543*, 15.

(3) Fleischmann, C.; Scherag, A.; Adhikari, N. K. J.; Hartog, C. S.; Tsaganos, T.; Schlattmann, P.; Angus, D. C.; Reinhart, K. Assessment of Global Incidence and Mortality of Hospital-Treated Sepsis Current Estimates and Limitations. *Am. J. Respir. Crit. Care Med.* **2016**, *193*, 259−272.

(4) Youkee, D.; Hulme, W.; Roberts, T.; Daniels, R.; Nutbeam, T.; Keep, J. Time Matters: Antibiotic Timing in Sepsis and Septic Shock. *Crit. Care Med.* **2016**, *44*, e1016−e1017.

(5) Jonasson, E.; Matuschek, E.; Kahlmeter, G. The EUCAST Rapid Disc Diffusion Method for Antimicrobial Susceptibility Testing Directly from Positive Blood Culture Bottles. *J. Antimicrob. Chemother.* **2020**, *75*, 968−978.

(6) van Belkum, A.; Dunne, W. M. Next-Generation Antimicrobial Susceptibility Testing. *J. Clin. Microbiol.* **2013**, *51*, 2018−2024.

(7) Schoepp, N. G.; Khorosheva, E. M.; Schlappi, T. S.; Curtis, M. S.; Humphries, R. M.; Hindler, J. A.; Ismagilov, R. F. Digital Quantification of DNA Replication and Chromosome Segregation Enables Determination of Antimicrobial Susceptibility after Only 15 Minutes of Antibiotic Exposure. *Angew. Chem., Int. Ed.* **2016**, *55*, 9557−9561.

(8) Hu, C.; Kalsi, S.; Zeimpekis, I.; Sun, K.; Ashburn, P.; Turner, C.; Sutton, J. M.; Morgan, H. Ultra-Fast Electronic Detection of Antimicrobial Resistance Genes Using Isothermal Amplification and Thin Film Transistor Sensors. *Biosens. Bioelectron.* **2017**, *96*, 281−287.

(9) Schoepp, N. G.; Schlappi, T. S.; Curtis, M. S.; Butkovich, S. S.; Miller, S.; Humphries, R. M.; Ismagilov, R. F. Rapid Pathogen-Specific Phenotypic Antibiotic Susceptibility Testing Using Digital LAMP Quantification in Clinical Samples. *Sci. Transl. Med.* **2017**, *9*, No. eaal3693.

(10) Notomi, T.; Mori, Y.; Tomita, N.; Kanda, H. Loop-Mediated Isothermal Amplification (LAMP): Principle, Features, and Future Prospects. *J. Microbiol.* **2015**, *53*, 1−5.

(11) Park, K.; Jeong, J.; Yi, S. Y.; Lee, W. S.; Shin, Y.-B. FRET Probe-Based Antibacterial Susceptibility Testing (F-AST) by Detection of Bacterial Nucleases Released by Antibiotic-Induced Lysis. *Biosens. Bioelectron.* **2019**, *130*, 225−229.

(12) Ellington, M. J.; Ekelund, O.; Aarestrup, F. M.; Canton, R.; Doumith, M.; Giske, C.; Grundman, H.; Hasman, H.; Holden, M. T. G.; Hopkins, K. L.; et al. The Role of Whole Genome Sequencing in Antimicrobial Susceptibility Testing of Bacteria: Report from the EUCAST Subcommittee. *Clin. Microbiol. Infect.* **2017**, *23*, 2−22.

(13) Bard, J. D.; Lee, F. Why Can't We Just Use PCR? The Role of Genotypic versus Phenotypic Testing for Antimicrobial Resistance Testing. *Clin. Microbiol. Newsl.* **2018**, *40*, 87−95.

(14) Dunne, W. M., Jr.; Jaillard, M.; Rochas, O.; Van Belkum, A. Microbial Genomics and Antimicrobial Susceptibility Testing. *Expert Rev. Mol. Diagn.* **2017**, *17*, 257−269.

(15) Fast antibiotic susceptibility results|Accelerate Pheno system.

(16) Baltekin, Ö.; Boucharin, A.; Tano, E.; Andersson, D. I.; Elf, J. Antibiotic Susceptibility Testing in Less than 30 Min Using Direct Single-Cell Imaging. *Proc. Natl. Acad. Sci. U.S.A.* **2017**, *114*, 9170−9175.

(17) Brennan-Krohn, T.; Smith, K. P.; Kirby, J. E. The Poisoned Well: Enhancing the Predictive Value of Antimicrobial Susceptibility Testing in the Era of Multidrug Resistance. *J. Clin. Microbiol.* **2017**, *55*, 2304−2308.

(18) Yu, H.; Jing, W.; Iriya, R.; Yang, Y.; Syal, K.; Mo, M.; Grys, T. E.; Haydel, S. E.; Wang, S.; Tao, N. Phenotypic Antimicrobial Susceptibility Testing with Deep Learning Video Microscopy. *Anal. Chem.* **2018**, *90*, 6314−6322.

(19) Syal, K.; Iriya, R.; Yang, Y.; Yu, H.; Wang, S.; Haydel, S. E.; Chen, H.-Y.; Tao, N. Antimicrobial Susceptibility Test with

Plasmonic Imaging and Tracking of Single Bacterial Motions on Nanometer Scale. *ACS Nano* **2016**, *10*, 845−852.
(20) Lissandrello, C.; Inci, F.; Francom, M.; Paul, M. R.; Demirci, U.; Ekinci, K. L. Nanomechanical Motion of Escherichia Coli Adhered to a Surface. *Appl. Phys. Lett.* **2014**, *105*, 113701.
(21) Gfeller, K. Y.; Nugaeva, N.; Hegner, M. Rapid Biosensor for Detection of Antibiotic-Selective Growth of Escherichia Coli. *Appl. Environ. Microbiol.* **2005**, *71*, 2626−2631.
(22) Bolotsky, A.; Ebrahimi, A. Toward Rapid Antibacterial Susceptibility Testing Using Electrochemical Biosensors Based on Organic−Inorganic Catalytic Complexes. *The 236th Electrochemical Society Meeting*; The Electrochemical Society, 2019; Vol. *MA2019-02*, p 2244.
(23) Besant, J. D.; Sargent, E. H.; Kelley, S. O. Rapid Electrochemical Phenotypic Profiling of Antibiotic-Resistant Bacteria. *Lab Chip* **2015**, *15*, 2799−2807.
(24) Johnson, W. L.; France, D. C.; Rentz, N. S.; Cordell, W. T.; Walls, F. L. Sensing Bacterial Vibrations and Early Response to Antibiotics with Phase Noise of a Resonant Crystal. *Sci. Rep.* **2017**, *7*, 12138.
(25) Resistell AG. Developing leading Rapid AST solution. https://resistell.com/ (accessed 08/27/2020).
(26) Jindal, S.; Thampy, H.; Day, P. J. R.; Kell, D. B. Very Rapid Flow Cytometric Assessment of Antimicrobial Susceptibility during the Apparent Lag Phase of Microbial (Re) Growth. *Microbiol.* **2019**, *165*, 439−454.
(27) Li, H.; Torab, P.; Mach, K. E.; Surrette, C.; England, M. R.; Craft, D. W.; Thomas, N. J.; Liao, J. C.; Puleo, C.; Wong, P. K. Adaptable Microfluidic System for Single-Cell Pathogen Classification and Antimicrobial Susceptibility Testing. *Proc. Natl. Acad. Sci. U.S.A.* **2019**, *116*, 10270−10279.
(28) Hayden, R. T.; Clinton, L. K.; Hewitt, C.; Koyamatsu, T.; Sun, Y.; Jamison, G.; Perkins, R.; Tang, L.; Pounds, S.; Bankowski, M. J. Rapid Antimicrobial Susceptibility Testing Using Forward Laser Light Scatter Technology. *J. Clin. Microbiol.* **2016**, *54*, 2701−2706.
(29) Draijer, M.; Hondebrink, E.; van Leeuwen, T.; Steenbergen, W. Review of Laser Speckle Contrast Techniques for Visualizing Tissue Perfusion. *Lasers Med. Sci.* **2009**, *24*, 639−651.
(30) Stoykova, E.; Kang, H.; Kim, Y.; Nazarova, D.; Nedelchev, L.; Ivanov, B.; Berberova, N.; Mateev, G. Evaluation of Activity from Binary Patterns in Dynamic Speckle Analysis. *Opt. Lasers Eng.* **2018**, *111*, 50−57.
(31) Murialdo, S. E.; Sendra, G. H.; Passoni, L. I.; Arizaga, R.; Gonzalez, J. F.; Rabal, H.; Trivi, M. Analysis of Bacterial Chemotactic Response Using Dynamic Laser Speckle. *J. Biomed. Opt.* **2009**, *14*, 064015.
(32) Ramírez-Miquet, E. E.; Cabrera, H.; Grassi, H. C.; Andrades, E. d. J.; Otero, I.; Rodríguez, D.; Darias, J. G. Digital Imaging Information Technology for Biospeckle Activity Assessment Relative to Bacteria and Parasites. *Lasers Med. Sci.* **2017**, *32*, 1375−1386.
(33) Yoon, J.; Lee, K.; Park, Y. A Simple and Rapid Method for Detecting Living Microorganisms in Food Using Laser Speckle Decorrelation. **2016**, arXiv:1603.07343.
(34) Ramírez-Miquet, E. E.; Cabrera, H.; Grassi, H. C.; Andrades, E. d. J.; Otero, I.; Rodríguez, D.; Darias, J. G. Digital Imaging Information Technology for Biospeckle Activity Assessment Relative to Bacteria and Parasites. *Lasers Med. Sci.* **2017**, *32*, 1375−1386.
(35) Hornik, K.; Stinchcombe, M.; White, H. Multilayer Feedforward Networks Are Universal Approximators. *Neural Networks* **1989**, *2*, 359−366.
(36) Rao, N. S. V.; Sen, S.; Liu, Z.; Kettimuthu, R.; Foster, I. Learning Concave-Convex Profiles of Data Transport over Dedicated Connections. *International Conference on Machine Learning for Networking*; Lecture Notes in Computer Science (Including Subseries Lecture Notes in Artificial Intelligence and Lecture Notes in Bioinformatics); Springer Verlag, 2019; Vol. *11407* LNCS, pp 1−22.
(37) Stetefeld, J.; McKenna, S. A.; Patel, T. R. Dynamic Light Scattering: A Practical Guide and Applications in Biomedical Sciences. *Biophys. Rev.* **2016**, *8*, 409−427.
(38) Li, L.; Mendis, N.; Trigui, H.; Oliver, J. D.; Faucher, S. P. The Importance of the Viable but Non-Culturable State in Human Bacterial Pathogens. *Front. Microbiol.* **2014**, *5*, 258.
(39) Satta, G.; Cornaglia, G.; Foddis, G.; Pompei, R. Evaluation of Ceftriaxone and Other Antibiotics against Escherichia Coli, Pseudomonas Aeruginosa, and Streptococcus Pneumoniae under in Vitro Conditions Simulating Those of Serious Infections. *Antimicrob. Agents Chemother.* **1988**, *32*, 552−560.
(40) Clinical & Laboratory Standards Institute. *CLSI Guidelines*, 2015; Vol. *32*, Number 3.
(41) Fredborg, M.; Andersen, K. R.; Jørgensen, E.; Droce, A.; Olesen, T.; Jensen, B. B.; Rosenvinge, F. S.; Sondergaard, T. E. Real-Time Optical Antimicrobial Susceptibility Testing. *J. Clin. Microbiol.* **2013**, *51*, 2047−2053.
(42) Choi, J.; Jeong, H. Y.; Lee, G. Y.; Han, S.; Han, S.; Jin, B.; Lim, T.; Kim, S.; Kim, D. Y.; Kim, H. C.; et al. Direct, Rapid Antimicrobial Susceptibility Test from Positive Blood Cultures Based on Microscopic Imaging Analysis. *Sci. Rep.* **2017**, *7*, 1148.
(43) Kalashnikov, M.; Mueller, M.; McBeth, C.; Lee, J. C.; Campbell, J.; Sharon, A.; Sauer-Budge, A. F. Rapid Phenotypic Stress-Based Microfluidic Antibiotic Susceptibility Testing of Gram-Negative Clinical Isolates. *Sci. Rep.* **2017**, *7*, 8031.
(44) Smith, K. P.; Richmond, D. L.; Brennan-Krohn, T.; Elliott, H. L.; Kirby, J. E. Development of MAST: A Microscopy-Based Antimicrobial Susceptibility Testing Platform. *SLAS Technol. Transl. Life Sci. Innovation* **2017**, *22*, 662−674.
(45) Villalba, M. I.; Stupar, P.; Chomicki, W.; Bertacchi, M.; Dietler, G.; Arnal, L.; Vela, M. E.; Yantorno, O.; Kasas, S. Nanomotion Detection Method for Testing Antibiotic Resistance and Susceptibility of Slow-Growing Bacteria. *Small* **2018**, *14*, 1702671.
(46) Stupar, P.; Opota, O.; Longo, G.; Prod'hom, G.; Dietler, G.; Greub, G.; Kasas, S. Nanomechanical Sensor Applied to Blood Culture Pellets: A Fast Approach to Determine the Antibiotic Susceptibility against Agents of Bloodstream Infections. *Clin. Microbiol. Infect.* **2017**, *23*, 400−405.
(47) Automated inoculum preparation for AST from crude samples. https://www.qlinea.com/0986741_wp-uploads/2020/01/Poster-ECCMID-2019-P1759.pdf (accessed 08/27/2020).
(48) Wistrand-Yuen, P.; Malmberg, C.; Fatsis-Kavalopoulos, N.; Lübke, M.; Tängdén, T.; Kreuger, J. A High-Throughput Fluidic Chip for Rapid Phenotypic Antibiotic Susceptibility Testing. **2019**, bioRxiv:647909.
(49) Flentie, K.; Spears, B. R.; Chen, F.; Purmort, N. B.; DaPonte, K.; Viveiros, E.; Phelan, N.; Krebill, C.; Flyer, A. N.; Hooper, D. C.; et al. Microplate-Based Surface Area Assay for Rapid Phenotypic Antibiotic Susceptibility Testing. *Sci. Rep.* **2019**, *9*, 237.
(50) Bugrysheva, J. V.; Lascols, C.; Sue, D.; Weigel, L. M. Rapid Antimicrobial Susceptibility Testing of Bacillus Anthracis, Yersinia Pestis, and Burkholderia Pseudomallei by Use of Laser Light Scattering Technology. *J. Clin. Microbiol.* **2016**, *54*, 1462−1471.

https://dx.doi.org/10.1021/acssensors.0c01238
ACS Sens. 2020, 5, 3140−3149